

## The (in)stability of functional brain network measures across thresholds



Kathleen A. Garrison<sup>a,\*</sup>, Dustin Scheinost<sup>b</sup>, Emily S. Finn<sup>c</sup>, Xilin Shen<sup>b</sup>, R. Todd Constable<sup>b,d</sup>

<sup>a</sup> Department of Psychiatry, Yale School of Medicine, USA

<sup>b</sup> Department of Diagnostic Radiology, Yale School of Medicine, USA

<sup>c</sup> Interdepartmental Neuroscience Program, Yale University, USA

<sup>d</sup> Department of Neurosurgery, Yale School of Medicine, USA

### ARTICLE INFO

#### Article history:

Received 31 January 2015

Accepted 16 May 2015

Available online 27 May 2015

#### Keywords:

Network analysis

Graph theory

Functional connectivity

Resting state

Threshold

### ABSTRACT

The large-scale organization of the brain has features of complex networks that can be quantified using network measures from graph theory. However, many network measures were designed to be calculated on binary graphs, whereas functional brain organization is typically inferred from a continuous measure of correlations in temporal signal between brain regions. Thresholding is a necessary step to use binary graphs derived from functional connectivity data. However, there is no current consensus on what threshold to use, and network measures and group contrasts may be unstable across thresholds. Nevertheless, whole-brain network analyses are being applied widely with findings typically reported at an arbitrary threshold or range of thresholds. This study sought to evaluate the stability of network measures across thresholds in a large resting state functional connectivity dataset. Network measures were evaluated across absolute (correlation-based) and proportional (sparsity-based) thresholds, and compared between sex and age groups. Overall, network measures were found to be unstable across absolute thresholds. For example, the direction of group differences in a given network measure may change depending on the threshold. Network measures were found to be more stable across proportional thresholds. These results demonstrate that caution should be used when applying thresholds to functional connectivity data and when interpreting results from binary graph models.

© 2015 Elsevier Inc. All rights reserved.

### Introduction

The human brain is a large-scale system of functionally connected brain regions. This system can be modeled as a network, or graph, by dividing the brain into a set of regions, or “nodes,” and quantifying the strength of the connections between nodes, or “edges,” as the temporal correlation in their patterns of activity. Network analysis, a part of graph theory, provides a set of summary statistics that can be used to describe complex brain networks using a reduced number of observations that can be meaningfully compared between groups and/or related to behavior (Rubinov and Sporns, 2010). Recent studies have used this approach to characterize network properties as they relate to sex (Tian et al., 2011), age (Meunier et al., 2009), and cognition (Dosenbach et al., 2007), as well as in conditions such as addiction (Chanraud et al., 2011), Alzheimer's disease (Supekar et al., 2008), schizophrenia (Alexander-Bloch et al., 2013; Bassett et al., 2008), and others (Bassett and Bullmore, 2006).

Network analyses of functional connectivity data are commonly based on the blood oxygen level-dependent (BOLD) signal in functional magnetic resonance imaging (fMRI), but can also be derived from electroencephalography (EEG) or magnetoencephalography (MEG). For

example, network analysis of fMRI data was used to show that more efficient global information processing (characteristic path length) in resting state was related to high intelligence quotient (IQ; van den Heuvel et al., 2009). Another study used network analysis of MEG data to show that functional integration (characteristic path length) and functional segregation (clustering coefficient) were decreased in Alzheimer's disease (Stam et al., 2009).

However, a central challenge of applying network analysis to functional connectivity data is that many network measures were designed to be calculated on binary graphs in which connections are either present or not, whereas temporal correlations in fMRI signal are continuous from  $-1$  to  $1$ . The typical approach is to: (1) define  $n$  non-overlapping nodes across the brain using an anatomical atlas or a functional parcellation method where nodes have voxels with similar time courses; (2) estimate the network by computing the entries of the  $n$ -by- $n$  matrix representing the functional connections between node pairs, either by linear association such as correlation or by some other nonlinear measure such as mutual information; and (3) apply a threshold to produce an  $n$ -by- $n$  binary adjacency matrix representing the network edges and to remove weak connections (Bullmore and Sporns, 2009; Simpson et al., 2013). Thus a threshold is commonly applied to construct a binary graph from functional connectivity data.

The use of thresholded binary graphs is attractive because it facilitates the calculation of many network measures and reduces the

\* Corresponding author at: 1 Church Street, Room 730, New Haven, CT 06511, USA.  
E-mail address: [kathleen.garrison@yale.edu](mailto:kathleen.garrison@yale.edu) (K.A. Garrison).

computational burden of analyzing the graph. An alternative approach is to use weighted graphs that are not binary but instead allow edges to carry some sort of continuous weight value. With weighted graphs, all edges remain in the graph and any node is connected to every other node. However, some have argued that weighted graphs are not reasonable biological structures because brain regions have sparse anatomical connections only to other specific brain regions (Sporns, 2011). Weighted graphs are also less computationally efficient, especially in the analysis of large-scale networks such as voxel-based functional connectivity networks (Telesford et al., 2011); the overwhelming number of connections makes it difficult to extract meaningful information (Serrano et al., 2009).

To define binary graphs, the applied threshold is typically absolute (correlation-based) or sparsity-based (proportional). Each approach has advantages and disadvantages. Absolute thresholds set a value for the correlation coefficient between node pairs, above which they are considered connected and below which they are not. Proportional thresholds utilize a set percentage of the strongest connections (edges), such as the top 10% of correlation values in the network. For group comparisons, using a proportional threshold ensures that the networks in each group have the same number of nodes, or network size, and the same number of edges, or global degree. This allows for more meaningful comparisons of other network measures that rely on degree. However, proportional thresholds do not take into account absolute differences in correlation values, therefore information about overall group differences may be lost. Absolute thresholds retain this information, but may result in networks with different size or degree, or in a network that is connected in one group but disconnected in the other group. While a difference in node-connectedness between groups may be informative, it confounds the comparison of graph measures that vary significantly with degree (Alexander-Bloch et al., 2010). Moreover, absolute thresholds may be too large for low-average connectivity networks or too small for high-average connectivity networks, thus eliminating strong and significant connections or overemphasizing weak connections (van Wijk et al., 2010).

There is also no consensus in the literature as to what specific threshold should be used. A large range of absolute thresholds have been applied, from a correlation coefficient of  $r = 0.1$  (Buckner et al., 2009, supplement) to  $r = 0.8$  (Tomasi and Volkow, 2010, supplement). Likewise a range of proportional thresholds have been reported, from 5 to 40% (e.g., Fornito et al., 2010). In attempts to show that results are not sensitive to the choice of threshold, findings are often reported across a narrow range of thresholds (e.g., Cole et al., 2013, top 2–10%; van den Heuvel et al., 2009,  $r = 0.3–0.5$ ). However, this can lead to incomplete results or even misleading results if network properties are unstable across a larger range of thresholds, for example if there is a reversal of group differences in a network measure across thresholds (e.g., Scheinost et al., 2012). Lastly, even if a canonical threshold was determined and agreed upon, different preprocessing decisions such as whether to use global signal regression (GSR) may shift the distribution of correlations (Murphy et al., 2009), leading to binary graphs that are not comparable across studies.

Therefore, this study sought to characterize the (in)stability of network measures across thresholds. A large resting-state fMRI dataset was used to measure network properties across the full range of absolute and proportional thresholds. In addition, the effects of GSR on network measures across thresholds were tested in order to highlight how preprocessing decisions can influence the (in)stability of network measures.

## Methods

### Participants

One hundred right-handed individuals participated in the study. All participants provided written informed consent in accordance with the

Yale Human Investigations Committee at the Yale School of Medicine. The analyses included 50 males (age  $35 \pm 10$  years) and 50 females (age  $34 \pm 12$  years). 99 of these were from a prior dataset of 103 subjects (Scheinost et al., 2015), 4 of whom were not included because they did not complete all 8 runs, and 1 additional participant was scanned in order to have equal sex groups. A subset of the current sample was grouped by age as younger participants (age range 18–25 years, mean age  $22 \pm 3$  years) and older participants (age range 44–66 years, mean age  $51 \pm 6$  years). Age groups were selected as the youngest and oldest participants matched between-groups by gender, and were selected to have participants matched within-groups by age and gender. Younger participants included 10 males (age range 18–25 years, mean age  $23 \pm 3$  years) and 10 females (age range 18–25 years, mean age  $22 \pm 2$  years). Older participants included 10 males (age range 44–66 years, mean age  $51 \pm 6$  years) and 10 females (age range 44–63 years, mean age  $51 \pm 6$  years).

### Imaging parameters

Data were acquired on two identical Siemens 3 T Tim Trio MRI scanners, including a localizer, followed by a low-resolution sagittal scan for slice alignment and a T1-weighted axial-oblique scan using a conventional spin-echo imaging sequence parallel to the AC-PC (25 slices, TR = 420 ms, TE = 11 ms; bandwidth = 130 Hz/pixel, flip angle =  $90^\circ$ , slice thickness = 6 mm; FOV =  $200 \times 200$  mm, matrix =  $256 \times 256$ ). Resting-state functional data was then obtained at the same slice locations using a T2\*-weighted gradient-recalled single shot echo-planar imaging sequence (TR = 1550 ms, TE = 30 ms, flip angle =  $80^\circ$ , FOV =  $220 \times 220$  mm, matrix =  $64 \times 64$ , slice thickness = 6 mm). Participants were instructed to rest with their eyes open, not to think of anything in particular, and not to fall asleep. There were 8 functional runs of 240 volumes each. The first 6 volumes were discarded to ensure the magnetization had reached steady state. Following the functional runs a high-resolution anatomical scan was obtained using a magnetization-prepared rapid gradient-echo (MPRAGE) imaging sequence (TR = 2530 ms, TE = 2.77 ms, TI = 1100 ms, flip angle =  $7^\circ$ , resolution =  $1 \times 1 \times 1$  mm).

### Connectivity preprocessing

Images were corrected for slice timing with sinc interpolation and realigned for motion correction using SPM5 (<http://www.fil.ion.ucl.ac.uk/spm/software/spm5>). In order to preserve the boundaries of functional nodes, no spatial smoothing was applied. All further preprocessing steps used BioImage Suite ([www.bioimagesuite.org](http://www.bioimagesuite.org); Joshi et al., 2011). Several covariates of no interest were regressed from the data including linear and quadratic drift, six rigid-body motion parameters, mean white matter signal, and mean cerebrospinal fluid (CSF) signal. To test the effects of global signal regression (GSR), in an identical dataset the mean overall global signal was regressed. All images were temporally smoothed using a zero mean unit Gaussian filter with an approximate cutoff frequency of 0.12 Hz.

### Network construction

First, 278 nodes were defined by warping the functional brain atlas ([http://www.nitrc.org/frs/download.php/5785/shenetal\\_neuroimage2013\\_funcatlas.zip](http://www.nitrc.org/frs/download.php/5785/shenetal_neuroimage2013_funcatlas.zip); Shen et al., 2010; Shen et al., 2013) into single subject space via a concatenation of linear and non-linear registrations: The functional images were linearly registered to the T1 axial-oblique (2D anatomical) images. The 2D anatomical images were linearly registered to the MPRAGE (3D anatomical) images. The 3D anatomical images were non-linearly registered to the template brain. All transformations were calculated and combined into a single transform and inverted, in order to reduce interpolation error by warping the atlas to an individual brain with only one transformation.

All transformations were estimated using the intensity-based registration algorithms in Biolum Suite.

For each participant, pairwise correlation coefficients were computed for the time courses of each pair of nodes with data from all runs. To test the stability of network measures across runs, pairwise correlation coefficients were computed for the time courses of each pair of nodes with data from each of the 8 runs. The correlation values were normalized to z-scores using the Fisher transformation, resulting in a  $278 \times 278$  connectivity matrix. Because the matrices are Fisher-transformed correlations, no matrices have zero surviving edges. The connectivity matrices were then converted into a binary adjacency matrix by thresholding using Matlab ([www.mathworks.org](http://www.mathworks.org)). Negative correlations were not included in the calculation of binary networks. An absolute threshold ( $\tau_r$ ) was applied from  $\tau_r = 0-1$  at 0.01 intervals. Using a Matlab function from Brain Connectivity Toolbox (<https://sites.google.com/site/bctnet>; Rubinov and Sporns, 2010), a proportional threshold ( $\tau_p$ ) was applied from  $\tau_p = 0.01-0.99$  at 0.01 intervals.

### Comparing network measures

Network properties were calculated using Matlab functions from Brain Connectivity Toolbox, and included the commonly reported network-level measures: characteristic path length, global efficiency, transitivity, and modularity; and node-level measures: clustering coefficient, local efficiency, degree, betweenness centrality, and participation coefficient. Definitions are provided in Table 1 (also see: Rubinov and Sporns, 2010). For network measures based on distance, such as characteristic path length, disconnected nodes are removed from the calculation. For network measures based on the adjacency matrix, such as degree, disconnected nodes are assigned a value of 0 (Rubinov and Sporns, 2010).

To visualize the stability of network measures, a ‘survival curve’ was plotted to describe how the network measure changes with connection threshold, i.e., survival as a function of threshold. The network measure value can be estimated as a single point on the survival curve. Therefore, the shape of this curve can be used to provide a description of network measure stability across thresholds, for example a monotonic curve

**Table 1**  
Network measures (Bassett and Bullmore, 2006; Rubinov and Sporns, 2010).

Network-level measures	
Characteristic path length ( $L$ )	is the average shortest path length (i.e., the minimal number of edges that form a direct connection between two nodes) between all pairs of nodes in the network and is a measure of functional integration. A short $L$ indicates a more compact network and more efficient global information processing.
Global efficiency ( $E_{glob}$ )	is the average inverse shortest path length between all pairs of nodes in the network and is a measure of functional integration, and represents the functional efficiency of brain networks for information transmission between multiple parallel paths.
Transitivity ( $T$ )	is the ratio of triangles to triplets in the network, and is a measure of clustering or functional segregation.
Modularity ( $M$ )	quantifies how well the network can be subdivided into non-overlapping groups of nodes or modules and is a measure of functional segregation.
Node-level measures	
Clustering coefficient ( $C$ )	is a measure of the number of edges between a node's nearest neighbors or the fraction of triangles around a node, and is a measure of functional segregation. High $C$ represents clustered connectivity at the node.
Local efficiency ( $E_{loc}$ )	is the global efficiency computed on node neighborhoods, is related to $C$ , and is a measure of functional segregation.
Degree ( $d$ )	is the number of edges connected to a node, and provides information related to the centrality of a node by determining nodes with a large number of connections.
Betweenness centrality ( $CB$ )	is the fraction of all the shortest paths in the network that contain a given node. Nodes with high $CB$ participate in a large number of shortest paths and may connect distinct parts of the network.
Participation coefficient ( $P$ )	is a measure of the inter-modular connections of nodes and indicates centrality.

would indicate stability, whereas a U-shape would indicate instability. Survival curves are displayed for a range of thresholds from less to more conservative: 0–1 for absolute thresholds; 0.99–.01 for proportional thresholds. To test network measure stability across thresholds, independent t-tests were used to compare measures between sex groups or age groups at each threshold. Reversals in the direction of significant group differences across thresholds (‘sign reversals’) were also used as an index of instability. In addition, correlations between each measure and age across all 100 participants were computed. To test network measure stability across runs, repeated measures analyses of variance were used to test for an effect of run at each threshold. All analyses were performed on graphs derived with and without GSR. Statistical analyses were performed using SPSS 21 (<http://www-01.ibm.com/software/analytics/spss>) or Matlab, and a significance level of  $p < .05$ . All reported findings are significant at this level (specific thresholds are reported in Tables 2–3). Several example nodes are described.

Inline Supplementary Table S1 can be found online at <http://dx.doi.org/10.1016/j.neuroimage.2015.05.046>.

## Results

### Network-level measures

#### Characteristic path length ( $L$ )

**Absolute threshold.** The survival curve for  $L$  has an inverted V-shape without GSR, with the maximum shifted to a lower threshold with GSR (Figs. 1A–F).  $L$  was longer for females or males (depending on threshold) with and without GSR (Figs. 1A–B).  $L$  did not differ by age without GSR; with GSR,  $L$  was longer for younger participants and was negatively correlated with age (Figs. 1C–D; Inline Supplementary Figure S1). The shape of the survival curve for  $L$  was consistent across runs, although an effect of run was found with and without GSR (Figs. 1E–F).

Inline Supplementary Fig. S1 can be found online at <http://dx.doi.org/10.1016/j.neuroimage.2015.05.046>.

**Proportional threshold.** The survival curve for  $L$  increases smoothly without GSR, or is flat and then increases smoothly with GSR (Figs. 1G–L).  $L$  was longer for males with and without GSR (Figs. 1G–H).  $L$  did not differ between age groups without GSR, yet was negatively or positively correlated with age; with GSR,  $L$  did not differ between age groups, yet was negatively correlated with age (Figs. 1I–J, Inline Supplementary Figure S1). The shape of the survival curve for  $L$  was consistent across runs, although an effect of run was found with and without GSR (Figs. 1K–L).

#### Global efficiency ( $E_{glob}$ )

**Absolute threshold.** The survival curve for  $E_{glob}$  is monotonic and decreases without GSR, with the minimum shifted to a lower threshold with GSR (Inline Supplementary Figures S2A–F).  $E_{glob}$  was higher for males with and without GSR (Inline Supplementary Figures. S2A–B).  $E_{glob}$  did not differ by age with or without GSR (Inline Supplementary Figures S2C–D, Inline Supplementary Figure S1). The shape of the survival curve for  $E_{glob}$  was consistent across runs, although an effect of run was found with and without GSR (Inline Supplementary Figures S2E–F).

Inline Supplementary Fig. S2 can be found online at <http://dx.doi.org/10.1016/j.neuroimage.2015.05.046>.

**Proportional threshold.** The survival curve for  $E_{glob}$  is monotonic and decreases without GSR, or is flat and then decreases with GSR (Inline Supplementary Figures S2G–L).  $E_{glob}$  did not differ between sex groups without GSR; with GSR,  $E_{glob}$  was higher for females (Inline Supplementary Figures S2G–H).  $E_{glob}$  did not differ between age groups without

**Table 2**  
Summary of significant group differences across thresholds.

	Metric	Absolute thresholds				Proportional thresholds			
		No GSR		GSR		No GSR		GSR	
		$T_r$	$T_r$	$T_r$	$T_r$	$T_p$	$T_p$	$T_p$	$T_p$
Sex group differences	<i>L</i>	F	0.34–0.82	F	0.04–0.09, 0.24–0.57	M	0.28–0.38	M	0.03, 0.05–0.38
	$E_{glob}$	M	0.92–1	M	0.73–0.75, 0.82–0.88, 0.94–0.98				
	<i>T</i>	M	0.37–0.98	M	0.03–0.95, 0.97			F	0.04–0.27
		M	0.21–0.42	M	0–0.34			M	0.04–0.99
		F	0.64–1	F	0.63–0.89			M	0.06–0.99
				M	0–0.02, 0.92–0.93, 0.96–0.97				
				F	0.41, 0.66, 0.69				
	Node								
	15	M	0.08, 0.1–0.29, 0.31–0.33	M	0.02–0.25	M	0.15, 0.23–0.24, 0.29–0.5	M	0.01, 0.08–0.39, 0.41
	272	F	0.59–0.75, 0.77, 0.79, 0.9	F	0.57–0.58, 0.61–0.65	M	0.71–0.82, 0.86, 0.88–0.93	M	0.17–0.99
Age group differences	$E_{loc}$	M	0.03–0.07, 0.1–0.24	M	0–0.17	M	0.01–0.05	F	0.01–0.05
	<i>d</i>	F	0.71–0.73	F	0.05–0.25	F	0.03–0.05, 0.07–0.99	M	0.3–0.36
				F	0.49–0.71	F	0.02–0.16, 0.18, 0.21–0.29	M	0.01
	104	F	0–0.70, 0.74–0.75, 0.81	F	0.64, 0.66–0.75, 0.81–0.89	M	0.02	F	0.11, 0.13, 0.28–0.39
		M	0.96, 0.98	M	0.18, 0.21–0.37, 0.39, 0.41–0.45, 0.48	M	0.09–0.1, 0.16, 0.2–0.23, 0.25, 0.27–0.36, 0.38–0.42, 0.44–0.48, 0.54–0.71, 0.77–0.81	M	0.01
	20	F	0.07–0.08, 0.17, 0.19–0.25, 0.4, 0.53–0.54	F	0.71, 0.73, 0.77, 0.8, 0.82–0.83	F		F	0.06–0.18, 0.28, 0.3, 0.32–0.33
		M	0.67, 0.69, 0.93	M					
	<i>L</i>			Younger	0.69, 0.71–0.72, 0.75–0.76, 0.89, 0.91–0.92				
	$E_{glob}$								
	<i>T</i>								
Age group differences	<i>M</i>	Younger	0.98	Younger	0.52, 0.54, 0.68, 0.70, 0.76, 0.83, 0.88	Younger	0.03–0.09, 0.12	Younger	0.05–0.06
	Node								
	174	Older	0.29	Older	0.04–0.29, 0.31	Older	0.28–0.39, 0.41, 0.43, 0.45–0.46, 0.48–0.49, 0.51–0.53, 0.57–0.58	Older	0.16, 0.18–0.39
		Younger	0.76–0.79	Younger	0.63–0.69	Older	0.28–0.31		
	128	Older	0.33–0.34, 0.4	Younger	0.64, 0.66–0.69	Older			
		Younger	0.66	Younger					
	199	Younger	0–0.11	Older	0.23–0.28, 0.34–0.37, 0.39–0.46	Older	0.04–0.05, 0.14	Older	0.04–0.08
		Older	0.55–0.65	Older		Younger	0.63–0.99	Younger	0.03
	26	Older	0.16–0.25, 0.36	Older	0.1	Older	0.17, 0.19–0.22, 0.34–0.57	Younger	
		Younger	0.75–0.76	Younger	0.61	Younger		Younger	
62	Younger	0.01–0.1, 0.19–0.32	Younger	0–0.07	Younger	0.01, 0.28–0.37, 0.39–0.41, 0.52–0.53, 0.75–0.76, 0.78–0.8, 0.82–0.83, 0.85, 0.88–0.89	Younger	0.25, 0.32, 0.35–0.99	
	Older	0.77, 0.93	Older						

*L* – characteristic path length,  $E_{glob}$  – global efficiency, *T* – transitivity, *M* – modularity, *C* – clustering coefficient,  $E_{loc}$  – local efficiency, *d* – degree, *CB* – betweenness centrality, *P* – participation coefficient, *M* – males, *F* – females;  $T_r$  – absolute threshold,  $T_p$  – proportional threshold; all results significant at  $p < .05$ .

**Table 3**  
Summary of significant effects of run across thresholds.

Effect of run	Metric	Absolute thresholds ( $\tau_r$ )		Proportional thresholds ( $\tau_p$ )	
		No GSR	GSR	No GSR	GSR
Effect of run	$L$	0.37–0.56	0.16–0.62, 0.93	0.06–0.53, 0.55, 0.59, 0.64, 0.82–0.92	0.02–0.03
	$E_{glob}$	0.54–0.86, 0.97–0.98	0.16–0.78	0.03–0.37, 0.82–0.91	
	$T$	0–0.47, 0.91–1		0.14–0.99	
	$M$	0.65, 0.69, 0.71	0.56, 0.71, 0.76, 0.78, 0.85		0.05

$L$  – characteristic path length,  $E_{glob}$  – global efficiency,  $T$  – transitivity,  $M$  – modularity; all results significant at  $p < .05$ .

GSR, yet was negatively correlated with age; with GSR,  $E_{glob}$  did not differ between age groups, yet was positively correlated with age (Inline Supplementary Figures S2I–J, Inline Supplementary Figure S1). The shape of the survival curve for  $E_{glob}$  was consistent across runs, although an effect of run was found without GSR (Inline Supplementary Figures S2K–L).

*Transitivity (T)*

**Absolute threshold.** The survival curve for  $T$  is U-shaped without GSR, with the minimum shifted to a lower threshold and J-shaped with GSR (Inline Supplementary Figures S3A–F).  $T$  was higher for males or

females with and without GSR (Inline Supplementary Figures S3A–B).  $T$  did not differ between age groups without GSR, yet was positively correlated with age; with GSR,  $T$  did not differ by age (Inline Supplementary Figures S3C–D, Inline Supplementary Figure S1). The shape of the survival curve for  $T$  was consistent across runs, although an effect of run was found without GSR (Inline Supplementary Figures S3E–F).

Inline Supplementary Fig. S3 can be found online at <http://dx.doi.org/10.1016/j.neuroimage.2015.05.046>.

**Proportional threshold.** The survival curve for  $T$  is monotonic and decreases without GSR, or is flat and then decreases with GSR (Inline

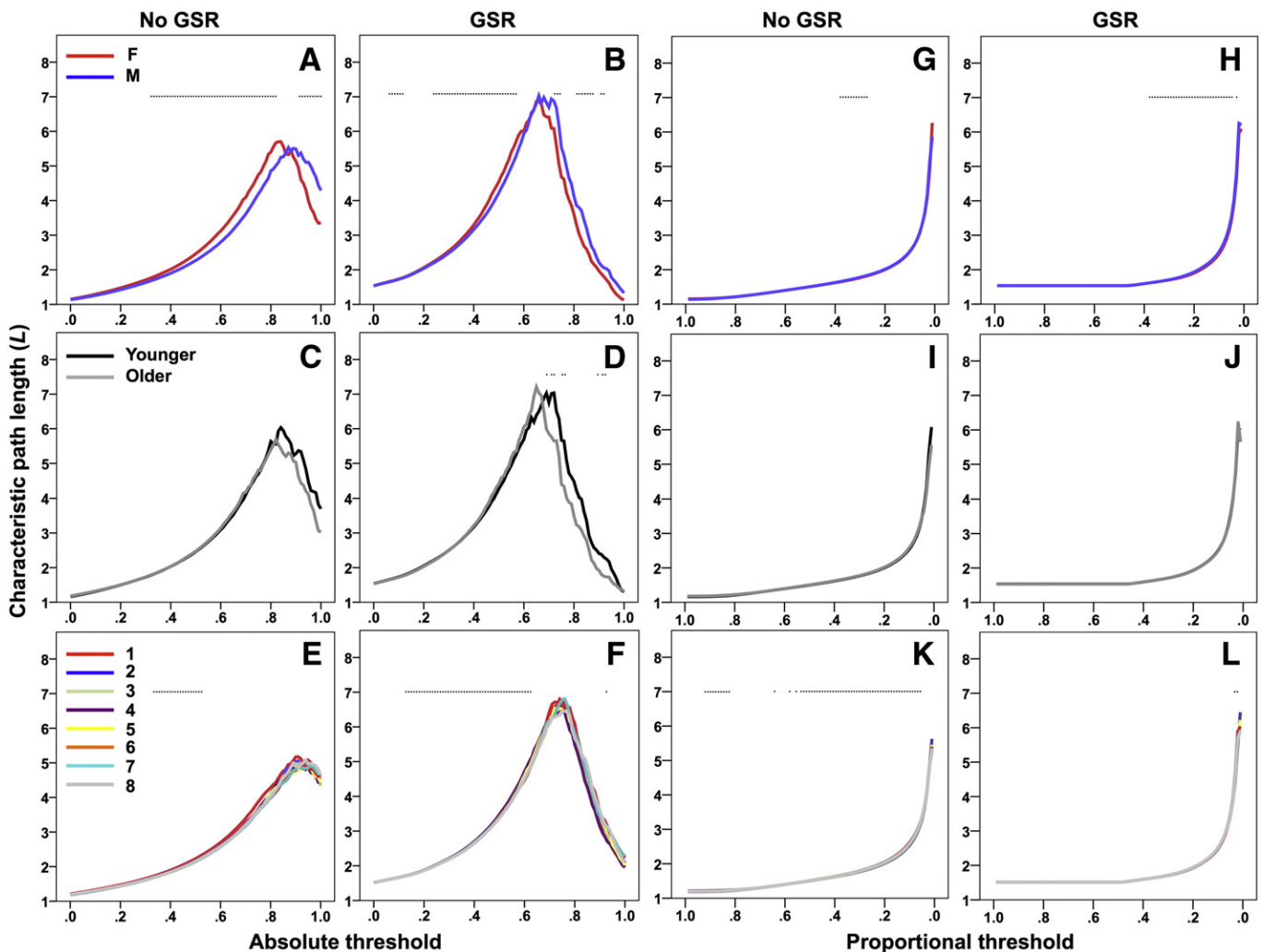


**Fig. 1.** Characteristic path length ( $L$ ) across absolute (A–F) and proportional (G–L) thresholds, compared between sex groups (top), age groups (middle), and across runs (bottom), without and with GSR. \* $p < .05$  (see Table 2).

Supplementary Figures S3G–L).  $T$  did not differ between sex groups without GSR; with GSR,  $T$  was higher for males (Inline Supplementary Figures S3G–H).  $T$  did not differ between age groups without GSR, yet was positively correlated with age; with GSR,  $T$  did not differ by age (Inline Supplementary Figures S3I–J, Inline Supplementary Figure S1). The shape of the survival curve for  $T$  was consistent across runs, although an effect of run was found without GSR (Inline Supplementary Figures S3K–L).

#### Modularity ( $M$ )

**Absolute threshold.** The survival curve for  $M$  is S-shaped without GSR, with the maximum shifted to a lower threshold and inverted J-shaped with GSR (Inline Supplementary Figures S4A–F).  $M$  did not differ between sex groups without GSR; with GSR,  $M$  was higher for males or females (Inline Supplementary Figures S4A–B).  $M$  was higher for younger participants without GSR and negatively correlated with age; with GSR,  $M$  was higher for younger participants and negatively

correlated with age (Inline Supplementary Figures S4C–D, Inline Supplementary Figure S1). The shape of the survival curve for  $M$  was consistent across runs, although an effect of run was found with and without GSR (Inline Supplementary Figures S4E–F).

Inline Supplementary Fig. S4 can be found online at <http://dx.doi.org/10.1016/j.neuroimage.2015.05.046>.

**Proportional threshold.** The survival curve for  $M$  increases smoothly to a final sharp peak without GSR, or is flat and then increases to a sharp peak with GSR (Inline Supplementary Figures S4G–L).  $M$  did not differ between sex groups without GSR; with GSR,  $M$  was higher for males (Inline Supplementary Figures S4G–H).  $M$  was higher for younger participants without GSR and negatively correlated with age; with GSR,  $M$  was higher for younger participants and negatively correlated with age (Inline Supplementary Figures S4I–J, Inline Supplementary Figure S1). The shape of the survival curve for  $M$  was consistent across runs, although an effect of run was found with GSR (Inline Supplementary Figures S4K–L).

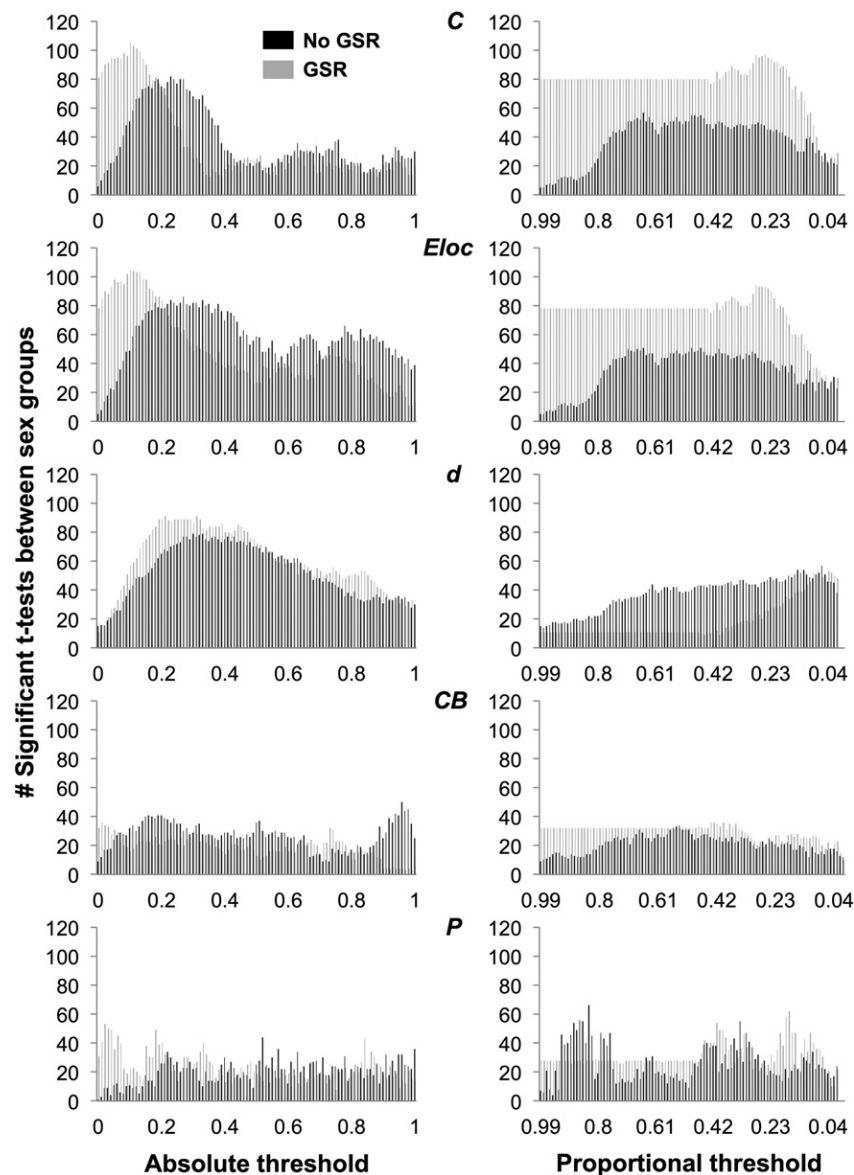


**Fig. 2.** Number of nodes showing a significant t-test between sex groups for clustering coefficient ( $C$ ), local efficiency ( $E_{loc}$ ), degree ( $d$ ), betweenness centrality ( $CB$ ), and participation coefficient ( $P$ ), across absolute thresholds (left) and proportional thresholds (right), without GSR (black) and with GSR (gray).  $p < .05$ .

Node-level measures

Clustering coefficient (*C*)

**Absolute threshold.** The number of nodes showing a difference in *C* between sex groups is skewed toward low thresholds without GSR, with the peak shifted toward lower thresholds with GSR (Fig. 2, left). Seventy-six nodes showed sign reversals between sex groups without GSR; 97 nodes showed sign reversals with GSR (Fig. 4). The survival curve for *C* is typically U- or S-shaped at a given node. At node 15, *C* was higher for males or females with and without GSR (Figs. 5A–B). The number of nodes showing a difference in *C* between age groups is minimal at low thresholds then increases without GSR, and higher at low thresholds and variable with GSR (Fig. 3, left). Twenty-two nodes showed sign reversals between age groups without GSR; 67 nodes showed sign reversals with GSR (Fig. 4). At node 174, *C* was higher for older or younger participants with and without GSR (Figs. 5E–F).

**Proportional threshold.** The number of nodes showing a difference in *C* between sex groups is minimal at high thresholds then increases

without GSR, and with GSR is flat and then peaks (Fig. 2). Three nodes showed sign reversals between sex groups without GSR; 5 nodes showed sign reversals with GSR (Fig. 4). The survival curve for *C* typically decreases or is stable and then drops off. At node 15, *C* was higher for males with and without GSR (Figs. 5C–D). The number of nodes showing a difference in *C* between age groups is minimal at high thresholds and variable without GSR, and with GSR is flat and then peaks (Fig. 3). Four nodes showed sign reversals between age groups without GSR; 2 nodes showed sign reversals with GSR (Fig. 4). At node 174, *C* was higher for older participants with and without GSR (Figs. 5G–H).

Local efficiency (*E<sub>loc</sub>*)

**Absolute threshold.** The number of nodes showing a difference in *E<sub>loc</sub>* between sex groups is skewed toward low thresholds without GSR, with the peak shifted toward lower thresholds with GSR (Fig. 2). Three nodes showed sign reversals between sex groups without GSR; 1 node showed a sign reversal with GSR (Fig. 4). The survival curve for *E<sub>loc</sub>* is typically non-monotonic with a downward trend. At node 272, *E<sub>loc</sub>* was higher for males or females with and without GSR (Inline

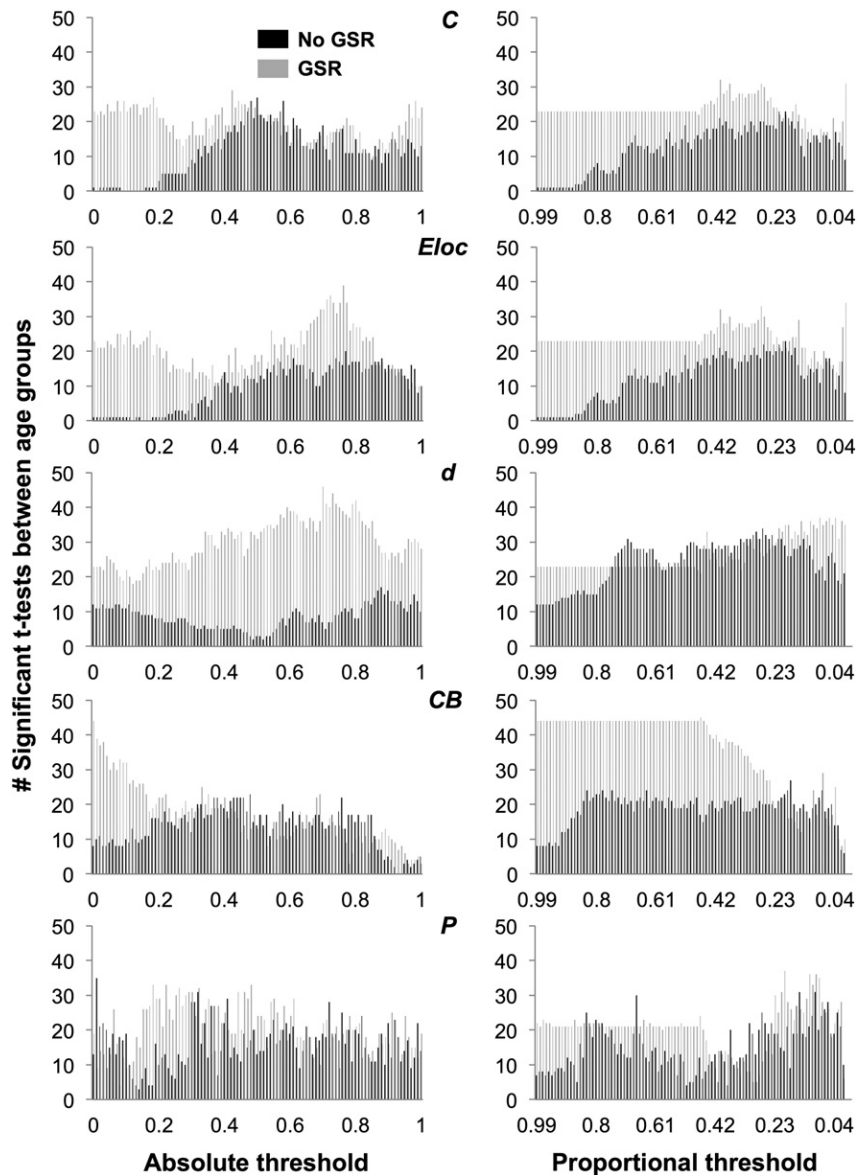


**Fig. 3.** Number of nodes showing a significant t-test between age groups for clustering coefficient (*C*), local efficiency (*E<sub>loc</sub>*), degree (*d*), betweenness centrality (*CB*), and participation coefficient (*P*), across absolute thresholds (left) and proportional thresholds (right), without GSR (black) and with GSR (gray). *p* < .05.

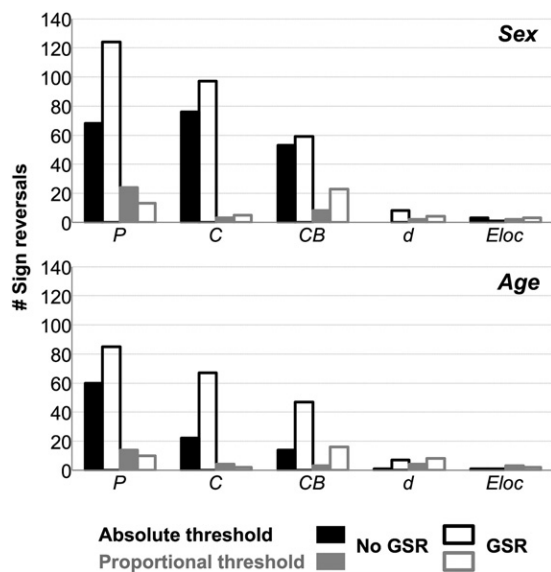


**Fig. 4.** Number of 'sign reversals' in the direction of significant differences for sex groups (top) and age groups, for participation coefficient ( $P$ ), clustering coefficient ( $C$ ), betweenness centrality ( $CB$ ), degree ( $d$ ), and local efficiency ( $E_{loc}$ ), across absolute thresholds (black) and proportional thresholds (gray), without GSR (solid bars) and with GSR (open bars).

Supplementary Figures S5A–B). The number of nodes showing a difference in  $E_{loc}$  between age groups is minimal at high thresholds then increases without GSR, and is higher at low thresholds and then peaks

with GSR (Fig. 3). One node showed a sign reversal between age groups with or without GSR (Fig. 4). At node 128,  $E_{loc}$  was higher for older or younger participants without GSR, and higher for younger participants with GSR (Inline Supplementary Figures S5E–F).

Inline Supplementary Fig. S5 can be found online at <http://dx.doi.org/10.1016/j.neuroimage.2015.05.046>.

**Proportional threshold.** The number of nodes showing a difference in  $E_{loc}$  between sex groups is minimal at high thresholds then increases without GSR, and with GSR is flat and then peaks (Fig. 2). Two nodes showed sign reversals between sex groups without GSR; 3 nodes showed sign reversals with GSR (Fig. 4). The survival curve for  $E_{loc}$  is typically non-monotonic and decreasing or is flat with a peak and drop-off. At node 272,  $E_{loc}$  was higher for males with and without GSR (Inline Supplementary Figures S5C–D). The number of nodes showing a difference in  $E_{loc}$  between age groups is minimal at high thresholds then increases without GSR, and with GSR is flat and then peaks (Fig. 3). Three nodes showed sign reversals between age groups without GSR; 2 nodes showed sign reversals with GSR (Fig. 4). At node 128,  $E_{loc}$  was higher for older participants without GSR (Inline Supplementary Figures S5G–H).

**Degree ( $d$ )**

**Absolute threshold.** The number of nodes showing a difference in  $d$  between sex groups is skewed toward low thresholds without GSR, with the peak shifted toward a slightly lower threshold with GSR (Fig. 2). No nodes showed a sign reversal between sex groups without GSR; 8 nodes showed sign reversals with GSR (Fig. 4). The survival curve for

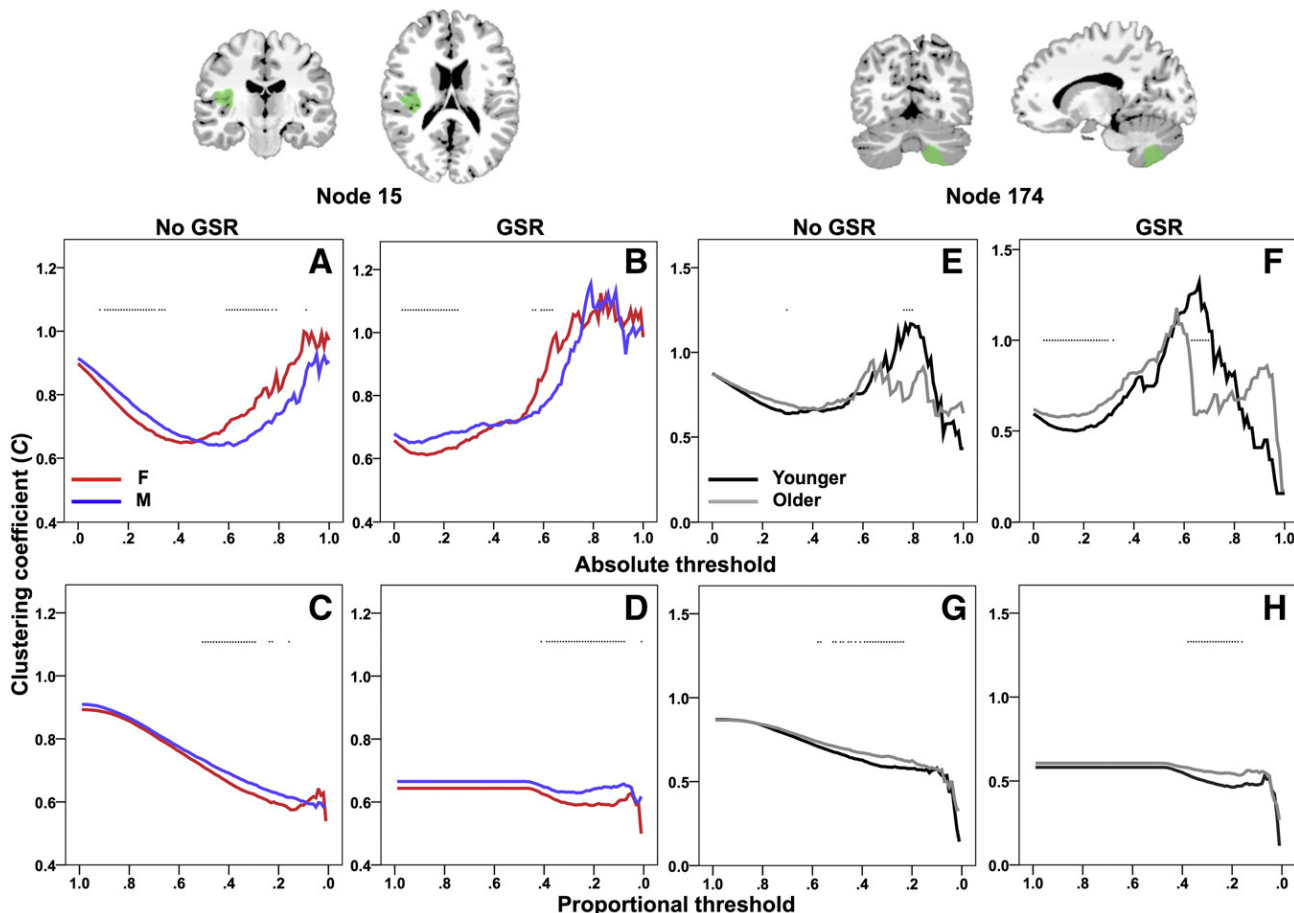


**Fig. 5.** Clustering coefficient ( $C$ ) compared between sex groups at node 15, and between age groups at node 174, across absolute thresholds (top) and proportional thresholds (bottom), without and with GSR. \* $p < .05$  (see Table 2). Node displayed (green) as overlay on MNI brain.

$d$  is typically monotonic and decreasing. At node 249,  $d$  did not show a difference between sex groups without GSR, but was higher for males or females with GSR (Inline Supplementary Figures S6A–B). The number of nodes showing a difference in  $d$  between age groups is variable without GSR, and is higher and skewed toward high thresholds with GSR (Fig. 3). One node showed a sign reversal between age groups without GSR; 7 nodes showed sign reversals with GSR (Fig. 4). At node 199,  $d$  was higher for younger or older participants without GSR, and higher for older participants with GSR (Inline Supplementary Figures S6E–F).

Inline Supplementary Fig. S6 can be found online at <http://dx.doi.org/10.1016/j.neuroimage.2015.05.046>.

**Proportional threshold.** The number of nodes showing a difference in  $d$  between sex groups increases without GSR, and with GSR is flat and then increases to peak (Fig. 2). Two nodes showed sign reversals between sex groups without GSR; 4 nodes showed sign reversals with GSR (Fig. 4). The survival curve for  $d$  is typically monotonic and decreasing or flat and then decreasing. At node 249,  $d$  was higher for females without GSR, and higher for females or males with GSR (Inline Supplementary Figures S6C–D). The number of nodes showing a difference in  $d$  between age groups was variable and increasing without GSR, and with GSR is flat and then peaks (Fig. 3). Four nodes showed sign reversals between age groups without GSR; 8 nodes showed sign reversals with GSR (Fig. 4). At node 199,  $d$  was higher for older or younger participants without GSR, and higher for older participants with GSR (Inline Supplementary Figures S6G–H).

#### Betweenness centrality (CB)

**Absolute threshold.** The number of nodes showing a difference in CB between sex groups is low and variable with or without GSR (Fig. 2). Fifty-three nodes showed sign reversals between sex groups without GSR; 59 nodes showed sign reversals with GSR (Fig. 4). The survival curve for CB is typically non-monotonic with an inverted V-shape. At node 104, CB was higher for females or males with and without GSR (Inline Supplementary Figures S7A–B). The number of nodes showing a difference in CB between age groups was highest at moderate thresholds without GSR, and skewed toward low thresholds with GSR (Fig. 3). Fourteen nodes showed sign reversals between age groups without GSR; 47 nodes showed sign reversals with GSR (Fig. 4). At node 26, CB was higher for older or younger participants with and without GSR (Inline Supplementary Figures S7E–F).

Inline Supplementary Fig. S7 can be found online at <http://dx.doi.org/10.1016/j.neuroimage.2015.05.046>.

**Proportional threshold.** The number of nodes showing a difference in CB between sex groups is low and variable without GSR, and with GSR is flat and then peaks (Fig. 2). Eight nodes showed sign reversals between sex groups without GSR; 23 nodes showed sign reversals with GSR (Fig. 4). The survival curve for CB typically increases to a sharp peak and then drops off. At node 104, CB was higher for females without GSR, and higher for males or females with GSR (Inline Supplementary Figures S7C–D). The number of nodes showing a difference in CB between age groups is variable without GSR, and with GSR is higher and flat and then peaks and decreases (Fig. 3). Three nodes showed sign reversals between age groups without GSR; 16 nodes showed sign reversals with GSR (Fig. 4). At node 26, CB was higher for older participants without GSR, and higher for younger participants with GSR (Inline Supplementary Figures S7G–H).

#### Participation coefficient (P)

**Absolute threshold.** The number of nodes showing a difference in  $P$  between sex groups is low and variable with and without GSR (Fig. 2). Sixty-eight nodes showed sign reversals between sex groups without GSR; 124 nodes showed sign reversals with GSR (Fig. 4). The survival

curve for  $P$  is typically non-monotonic with a downward trend. At node 20,  $P$  was higher for females or males with or without GSR (Inline Supplementary Figures S8A–B). The number of nodes showing a difference in  $P$  between age groups is variable with and without GSR (Fig. 3). Sixty nodes showed sign reversals between age groups without GSR; 85 nodes showed sign reversals with GSR (Fig. 4). At node 62,  $P$  was higher for younger or older participants without GSR, and higher for younger participants with GSR (Inline Supplementary Figures S8E–F).

Inline Supplementary Fig. S8 can be found online at <http://dx.doi.org/10.1016/j.neuroimage.2015.05.046>.

**Proportional threshold.** The number of nodes showing a difference in  $P$  between sex groups is variable without GSR, and with GSR is flat and then peaks (Fig. 2). Twenty-four nodes showed sign reversals between sex groups without GSR; 13 nodes showed sign reversals with GSR (Fig. 4). The survival curve for  $P$  is typically non-monotonic with an inverted J-shape or flat and then J-shaped. At node 20,  $P$  was higher for males or females with and without GSR (Inline Supplementary Figures S8C–D). The number of nodes showing a difference in  $P$  between age groups is variable without GSR, and with GSR is flat, drops off and then peaks (Fig. 3). Fourteen nodes showed sign reversals between age groups without GSR; 10 nodes showed sign reversals with GSR (Fig. 4). At node 62,  $P$  was higher for younger participants with and without GSR (Inline Supplementary Figures S8G–H).

## Discussion

Network measures were found to be unstable in a number of ways, particularly across absolute thresholds. Few of the survival curves were monotonic across absolute thresholds (e.g., Figs. 1A–F); this can make it difficult to parameterize the curve with a simple function (as in Scheinost et al., 2012). Most of the network measures showed ‘sign reversals’ in the direction of group differences across absolute thresholds (Fig. 4). Finally, the number of nodes showing a significant group difference in a given network measure across absolute thresholds was typically variable or skewed, i.e., not flat (Figs. 2–3).

$E_{glob}$  and  $M$  were the most stable network-level measures across absolute thresholds.  $E_{glob}$  is defined as the average inverse shortest path length (Rubinov and Sporns, 2010) and is therefore related to  $L$ . The current findings suggest that  $E_{glob}$  may be a more stable measure of functional integration than  $L$  when using absolute thresholds. Further, although  $E_{glob}$  exhibited a monotonic survival curve across absolute thresholds (Inline Supplementary Figures S2A–F), the curve for  $E_{loc}$  at a given node was typically non-monotonic across absolute thresholds (Inline Supplementary Figures S5A–B, E–F). This suggests that nodes may contribute to  $E_{glob}$  differently across absolute thresholds. The most stable node-level measures were  $d$  and  $E_{loc}$ , with few to no nodes showing sign reversals in these measures across absolute thresholds (Fig. 4). Only one node showed a sign reversal in  $d$  across absolute thresholds (node 199, Inline Supplementary Figures S6E).

The stability of network measures was improved using proportional thresholds. The survival curves for network measures across proportional thresholds had more smoothly varying shapes. For example, the inverted V-shaped curves of  $L$  across absolute thresholds were not found (Fig. 1). Although a few network measures showed sign reversals across proportional thresholds (Fig. 4), in each instance, the reversal occurred at one or a few extreme thresholds. For example, at node 20,  $P$  was higher for males at  $\tau_p = 0.01$  or  $0.02$ , but higher for females at virtually every other threshold (Inline Supplementary Figures S8C–D). The number of nodes showing a significant group difference in a network measure across proportional thresholds was also less variable or more flat (Figs. 2–3). These findings suggest that network measures are more stable across proportional than absolute thresholds. The application of proportional thresholds has become more common in graph theoretical analyses of human brain networks (e.g., Achard and

Bullmore, 2007; Zhang et al., 2011). However, these findings demonstrate that the outcome of network analyses can differ depending on whether absolute or proportional thresholds are applied. For example,  $E_{glob}$  was found to be greater for males than females across absolute thresholds, but greater for females than males across proportional thresholds, when the same preprocessing method was used (Inline Supplementary Figures S2B, H).

The instability of network measures at very high or very low thresholds is expected and is related to the calculation of these measures as the graph becomes more or less connected. The current findings demonstrate, however, that network measure instability is not restricted to extreme thresholds, but occurs within reasonable, commonly applied ranges. For instance,  $L$  decreases at high absolute thresholds (and also at very low proportional thresholds  $<.01$ ; not displayed) because many nodes no longer have paths between them that survive threshold, thereby decreasing the average shortest path length. However, the instability of  $L$  was not restricted to high absolute thresholds (Fig. 1). With GSR,  $L$  was greater for females at reportable, low thresholds ( $r = 0.24–0.57$ ), but greater for males at reportable, high thresholds ( $r = 0.73–0.75, 0.82–0.88$ ), as published studies have reported findings at absolute thresholds ranging from  $r = 0.1–0.8$  (e.g., Buckner et al., 2009; Tomasi and Volkow, 2010; supplements). For network measures showing sign reversals in the direction of group differences across absolute thresholds, most showed sign reversals within the typically reported range (Table 2). Proportional thresholds were found to improve network measure stability, and this was indicated by all sign reversals across proportional thresholds occurring at one or a few extreme thresholds, as described above.

Network measures were also found to be somewhat unstable within subjects across the eight resting-state fMRI runs. Only network-level measures were tested across runs. Although the shapes of the survival curves were consistent across runs (e.g., Figs. 1E–F, K–L), indicating relative stability, there was nevertheless a significant effect of run on every network measure at some thresholds, depending on the type of threshold applied and the preprocessing method.

Finally, these findings demonstrate an impact of preprocessing with GSR, but did not reveal a consistent effect of GSR on the stability of network measures. The survival curves were typically shifted by GSR across absolute or proportional thresholds. GSR impacted group differences in a number of ways: (a) group differences were only found with GSR (e.g., sex;  $E_{glob}$ ,  $T$ ,  $M$ ; proportional threshold); (b) group differences found without GSR were no longer found with GSR (e.g., age; node 128;  $E_{loc}$ ; proportional threshold); (c) sign reversals found without GSR resolved to one direction of group differences with GSR (e.g., age; node 199;  $d$ ; absolute or proportional threshold); and (d) at worst, the direction of group differences found without GSR reversed with GSR (e.g., age; node 26;  $CB$ ; proportional threshold). Across absolute thresholds, with GSR, all network measures showed a sign reversal by sex with the exception of  $E_{glob}$ . Across proportional thresholds, with GSR,  $d$ ,  $CB$ , and  $P$  showed sign reversals. These findings suggest that GSR does not improve network measure stability in any consistent way. It is possible that in some instances, the group differences found with GSR are a correct representation of the data. GSR may facilitate observations of true physiological relationships in the brain (Fox et al., 2009) and can help mitigate artifacts due to motion (Yan et al., 2013) or variations in carbon dioxide (Wise et al., 2004). However, in the current findings, it is not possible to determine whether GSR reveals true group differences, and overall, GSR was not found to stabilize network measures across thresholds. Alternative solutions to account for global signal fluctuations include physiological noise removal using independent components (Griffanti et al., 2014) or principal components analysis (e.g., CompCor; Behzadi et al., 2007).

In summary, network analyses enable characterization of the large-scale organization of the brain from fMRI connectivity data, however, a threshold is commonly applied to infer network structure from the data, and the current findings, and other studies (e.g., Scheinost et al.,

2012), have shown that network measures are unstable across thresholds. Here we provide additional evidence that network measures are unstable across runs and can change with different preprocessing pipelines. As there is no biologically principled way to set a threshold for a brain network, thresholds remain an ‘educated guess’ (Van Dijk et al., 2010). The current findings demonstrate that the choice of thresholding approach can dramatically impact results, including even reversing the direction of group differences in a network measure.

Recent studies have reported findings across a range of thresholds. This is useful for a more complete understanding of the data. Other approaches to thresholding were not tested in the current study, such as weighted graphs, in which edges carry some continuous weight value, such as related to the strength or effectiveness of connections, or the distance between nodes (Reijneveld et al., 2007). However, it is not straightforward how best to set weights that reflect the relative strengths of connections (Fornito et al., 2010). It has also been suggested that weighted graphs are not reasonable biological structures because in weighted graphs all brain regions are connected to all other brain regions (Sporns, 2011). However, unlike measures of anatomical connectivity which are considered to reflect direct connections, functional connectivity measures reflect both direct (monosynaptic) and indirect (polysynaptic) connections (Buckner et al., 2013), and therefore weighted graphs in which all nodes are connected may still reflect a reasonable representation of brain networks. Methods have improved for modeling weighted brain networks (e.g., Latora and Marchiori, 2003), and the weighted approach has been used to characterize network properties as they relate to sex and age (Gong et al., 2009), among others. Additional methods can be used that integrate network measures over a full range of thresholds and, thus, are not sensitive to threshold effects (e.g., Ginestet et al., 2011; Scheinost et al., 2012). One approach is to parameterize the distribution of a network measure calculated over all thresholds (Scheinost et al., 2012). These parameters can then be used to compare connectivity between groups (e.g., Garrison et al., 2014; Scheinost et al., 2015), or to relate connectivity to behavior or other variables (e.g., Mitchell et al., 2013). A second approach is to use Monte Carlo sampling to integrate network measures over a range of proportional thresholds for both weighted and unweighted networks (Ginestet et al., 2011).

## Conclusion

Network analyses are useful for summarizing large-scale brain organization, to relate features of network topology to behavior and cognition, and to examine changes in these features in clinical populations such as individuals with neurological and psychiatric disorders. However, caution must be used when conducting and interpreting network analyses. As studies work to elucidate the organization of functional brain networks in these and other contexts, the choice of thresholding approach must be carefully motivated because the network structure inferred largely determines the neurobiological interpretation (Rubinov and Sporns, 2010).

## Acknowledgments

We thank our research participants for their time and efforts. This work was funded by grants from the National Institutes of Health, National Institute on Drug Abuse (to KAG: K12DA00167; to DS: T32DA022975); the American Heart Association (to KAG: 14CRP18200010); and the National Science Foundation (to EF: Graduate Research Fellowship).

## References

- Achard, S., Bullmore, E., 2007. Efficiency and cost of economical brain functional networks. *PLoS Comput. Biol.* 3, e17.

- Alexander-Bloch, A.F., Gogtay, N., Meunier, D., Birn, R., Clasen, L., Lalonde, F., Lenroot, R., Giedd, J., Bullmore, E.T., 2010. Disrupted modularity and local connectivity of brain functional networks in childhood-onset schizophrenia. *Front. Syst. Neurosci.* 4, 147.
- Alexander-Bloch, A.F., Vertes, P.E., Stidd, R., Lalonde, F., Clasen, L., Rapoport, J., Giedd, J., Bullmore, E.T., Gogtay, N., 2013. The anatomical distance of functional connections predicts brain network topology in health and schizophrenia. *Cereb. Cortex* 23, 127–138.
- Bassett, D.S., Bullmore, E., 2006. Small-world brain networks. *Neuroscientist* 12, 512–523.
- Bassett, D.S., Bullmore, E., Verchinski, B.A., Mattay, V.S., Weinberger, D.R., Meyer-Lindenberg, A., 2008. Hierarchical organization of human cortical networks in health and schizophrenia. *J. Neurosci.* 28, 9239–9248.
- Behzadi, Y., Restom, K., Liu, J., Liu, T.T., 2007. A component based noise correction method (CompCor) for BOLD and perfusion based fMRI. *NeuroImage* 37, 90–101.
- Buckner, R.L., Sepulcre, J., Talukdar, T., Krienen, F.M., Liu, H., Hedden, T., Andrews-Hanna, J.R., Sperling, R.A., Johnson, K.A., 2009. Cortical hubs revealed by intrinsic functional connectivity: mapping, assessment of stability, and relation to Alzheimer's disease. *J. Neurosci.* 29, 1860–1873.
- Buckner, R.L., Krienen, F.M., Yeo, B.T., 2013. Opportunities and limitations of intrinsic functional connectivity MRI. *Nat. Neurosci.* 16, 832–837.
- Bullmore, E., Sporns, O., 2009. Complex brain networks: graph theoretical analysis of structural and functional systems. *Nat. Rev. Neurosci.* 10, 186–198.
- Chanraud, S., Pitel, A.L., Pfefferbaum, A., Sullivan, E.V., 2011. Disruption of functional connectivity of the default-mode network in alcoholism. *Cereb. Cortex* 21, 2272–2281.
- Cole, M.W., Reynolds, J.R., Power, J.D., Repovs, G., Anticevic, A., Braver, T.S., 2013. Multitask connectivity reveals flexible hubs for adaptive task control. *Nat. Neurosci.* 16, 1348–1355.
- Dosenbach, N.U., Fair, D.A., Miezin, F.M., Cohen, A.L., Wenger, K.K., Dosenbach, R.A., Fox, M.D., Snyder, A.Z., Vincent, J.L., Raichle, M.E., Schlaggar, B.L., Petersen, S.E., 2007. Distinct brain networks for adaptive and stable task control in humans. *Proc. Natl. Acad. Sci. U. S. A.* 104, 11073–11078.
- Fornito, A., Zalesky, A., Bullmore, E.T., 2010. Network scaling effects in graph analytic studies of human resting-state fMRI data. *Front. Syst. Neurosci.* 4, 22.
- Fox, M.D., Zhang, D., Snyder, A.Z., Raichle, M.E., 2009. The global signal and observed anticorrelated resting state brain networks. *J. Neurophysiol.* 101, 3270–3283.
- Garrison, K.A., Scheinost, D., Constable, R.T., Brewer, J.A., 2014. BOLD signal and functional connectivity associated with loving kindness meditation. *Brain Behav.* 4, 337–347.
- Ginestet, C.E., Nichols, T.E., Bullmore, E.T., Simmons, A., 2011. Brain network analysis: separating cost from topology using cost-integration. *PLoS ONE* 6, e21570.
- Gong, G., Rosa-Neto, P., Carbonell, F., Chen, Z.J., He, Y., Evans, A.C., 2009. Age- and gender-related differences in the cortical anatomical network. *J. Neurosci.* 29, 15684–15693.
- Griffanti, L., Salimi-Khorshidi, G., Beckmann, C.F., Auerbach, E.J., Douaud, G., Sexton, C.E., Zsoldos, E., Ebmeier, K.P., Filippini, N., Mackay, C.E., Moeller, S., Xu, J., Yacoub, E., Baselli, G., Ugurbil, K., Miller, K.L., Smith, S.M., 2014. ICA-based artefact removal and accelerated fMRI acquisition for improved resting state network imaging. *NeuroImage* 95, 232–247.
- Joshi, A., Scheinost, D., Okuda, H., Belhachemi, D., Murphy, I., Staib, L.H., Papademetris, X., 2011. Unified framework for development, deployment and robust testing of neuroimaging algorithms. *Neuroinformatics* 9, 69–84.
- Latora, V., Marchiori, M., 2003. Economic small world behavior in weighted networks. *Eur. Phys. J.* 32, 249–263.
- Meunier, D., Achard, S., Morcom, A., Bullmore, E., 2009. Age-related changes in modular organization of human brain functional networks. *NeuroImage* 44, 715–723.
- Mitchell, M.R., Balodis, I.M., Devito, E.E., Lacadie, C.M., Yeston, J., Scheinost, D., Constable, R.T., Carroll, K.M., Potenza, M.N., 2013. A preliminary investigation of Stroop-related intrinsic connectivity in cocaine dependence: associations with treatment outcomes. *Am. J. Drug Alcohol Abuse* 39, 392–402.
- Murphy, K., Birn, R.M., Handwerker, D.A., Jones, T.B., Bandettini, P.A., 2009. The impact of global signal regression on resting state correlations: are anti-correlated networks introduced? *NeuroImage* 44, 893–905.
- Reijneveld, J.C., Ponten, S.C., Berendse, H.W., Stam, C.J., 2007. The application of graph theoretical analysis to complex networks in the brain. *Clin. Neurophysiol.* 118, 2317–2331.
- Rubinov, M., Sporns, O., 2010. Complex network measures of brain connectivity: uses and interpretations. *NeuroImage* 52, 1059–1069.
- Scheinost, D., Benjamin, J., Lacadie, C.M., Vohr, B., Schneider, K.C., Ment, L.R., Papademetris, X., Constable, R.T., 2012. The intrinsic connectivity distribution: a novel contrast measure reflecting voxel level functional connectivity. *NeuroImage* 62, 1510–1519.
- Scheinost, D., Finn, E.S., Tokoglu, F., Shen, X., Papademetris, X., Hampson, M., Constable, R.T., 2015. Sex differences in normal age trajectories of functional brain networks. *Hum. Brain Mapp.* 36, 1524–1535.
- Serrano, M.A., Boguna, M., Vespignani, A., 2009. Extracting the multiscale backbone of complex weighted networks. *Proc. Natl. Acad. Sci. U. S. A.* 106, 6483–6488.
- Shen, X., Papademetris, X., Constable, R.T., 2010. Graph-theory based parcellation of functional subunits in the brain from resting-state fMRI data. *NeuroImage* 50, 1027–1035.
- Shen, X., Tokoglu, F., Papademetris, X., Constable, R.T., 2013. Groupwise whole-brain parcellation from resting-state fMRI data for network node identification. *NeuroImage* 82, 403–415.
- Simpson, S.L., Bowman, F.D., Laurienti, P.J., 2013. Analyzing complex functional brain networks: fusing statistics and network science to understand the brain. *Stat. Surv.* 7, 1–36.
- Sporns, O., 2011. *Networks of the Brain*. MIT Press, Cambridge, MA.
- Stam, C.J., de Haan, W., Daffertshofer, A., Jones, B.F., Manshanden, I., van Cappellen van Walsum, A.M., Montez, T., Verbunt, J.P., de Munck, J.C., van Dijk, B.W., Berendse, H.W., Scheltens, P., 2009. Graph theoretical analysis of magnetoencephalographic functional connectivity in Alzheimer's disease. *Brain* 132, 213–224.
- Supekar, K., Menon, V., Rubin, D., Musen, M., Greicius, M.D., 2008. Network analysis of intrinsic functional brain connectivity in Alzheimer's disease. *PLoS Comput. Biol.* 4, e1000100.
- Telesford, Q.K., Simpson, S.L., Burdette, J.H., Hayasaka, S., Laurienti, P.J., 2011. The brain as a complex system: using network science as a tool for understanding the brain. *Brain Connect.* 1, 295–308.
- Tian, L., Wang, J., Yan, C., He, Y., 2011. Hemisphere- and gender-related differences in small-world brain networks: a resting-state functional MRI study. *NeuroImage* 54, 191–202.
- Tomas, D., Volkow, N.D., 2010. Functional connectivity density mapping. *Proceedings of the National Academy of Sciences of the United States of America.* 107, pp. 9885–9890.
- van den Heuvel, M.P., Stam, C.J., Kahn, R.S., Hulshoff Pol, H.E., 2009. Efficiency of functional brain networks and intellectual performance. *J. Neurosci.* 29, 7619–7624.
- Van Dijk, K.R.A., Hedden, T., Venkataraman, A., Evans, K.C., Lazar, S.W., Buckner, R.L., 2010. Intrinsic functional connectivity as a tool for human connectomics: theory, properties, and optimization. *J. Neurophysiol.* 103, 297–321.
- van Wijk, B.C., Stam, C.J., Daffertshofer, A., 2010. Comparing brain networks of different size and connectivity density using graph theory. *PLoS ONE* 5, e13701.
- Wise, R.G., Ide, K., Poulin, M.J., Tracey, I., 2004. Resting fluctuations in arterial carbon dioxide induce significant low frequency variations in BOLD signal. *NeuroImage* 21, 1652–1664.
- Yan, C.G., Cheung, B., Kelly, C., Colcombe, S., Craddock, R.C., Di Martino, A., Li, Q., Zuo, X.N., Castellanos, F.X., Milham, M.P., 2013. A comprehensive assessment of regional variation in the impact of head micromovements on functional connectomics. *NeuroImage* 76, 183–201.
- Zhang, J., Wang, J., Wu, Q., Kuang, W., Huang, X., He, Y., Gong, Q., 2011. Disrupted brain connectivity networks in drug-naive, first-episode major depressive disorder. *Biol. Psychiatry* 70, 334–342.